Article

Superhydrophobic Multifocal Microlens Array with Depth-of-Field Detection for a Humid Environment

Hao Cao, Hongfeng Deng, Hui Wan, Shiyi Luan, Su Shen,* and Chengqun Gui*

Read Online

ACCESS | Metrics & More | Article Recommendations | Supporting Information

ABSTRACT: Microlens array (MLA) has been widely applied in augmented reality and optical imaging. When used in a humid environment or medical endoscopy, MLA needs to be both superhydrophobic and multifocal. However, it is not easy to achieve both superhydrophobic and multifocal function by integrating superhydrophobic and multifocal structures on the same surface by means of a simple, efficient, and precise method. In this paper, the superhydrophobic multifocal MLA with superhydrophobic properties and multifocal functions is successfully designed for preparation based on a method of 3D lithography and soft lithography. The 3D lithography can further help the preparation of a multifocal MLA with varying apertures and a multistep superhydrophobic structure with a round dome. The superhydrophobic multifocal MLA with periods 50 and 120 μm has perfect superhydrophobic property. The water droplet can slide and bounce off the surface at a roll angle of less than 12.9° with both multifocal and integrated imaging function, as well as up to 397 μm depth-of-field (DOF) detection range; this greatly exceeds the conventional MLA. The perfect superhydrophobic and optical property can be achieved in an extremely humid environment. The superhydrophobic multifocal MLA proposed in this paper has a promising prospect for actual practices.
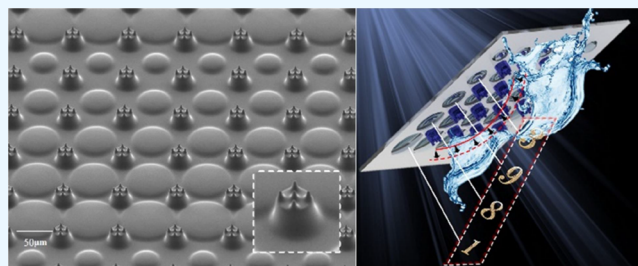
1. INTRODUCTION

Inspired by biological compound eyes, researchers have conducted many studies on microlens array (MLA) which has been widely applied in many fields including fiber-optic sensing, beam shaping, and medical endoscopic lens.[1−6] The rapid development of augmented reality (AR) and virtual reality (VR) technologies has further extended the applications into multiple fields such as our daily life and military aerospace,[7−11] and the MLA is also regarded as an indispensable micro-optical device within this system.[12−16] For the applications in different environments, especially outdoors, MLA needs to be added with some additional properties. For example, water droplets may adhere to the MLA in outdoor or humid environments and result in obviously less optical performance, in terms of imaging and light convergence. Then, it is urgently necessary to improve the MLA's water resistance.[17] Moreover, when the medical endoscope is used in surgery, the fluid environment inside the human body will bring a greater impact on the imaging effect, so it is also urgently necessary to enable it with the waterproof property. Meanwhile, it is also hoped to detect further information on the cellular tissues in the lesion area, so it is necessary to enable it with the function of depth-of-field (DOF) detection.[18,19]

The MLA requires less surface roughness for optical performance, whereas the hydrophobic structure, especially the superhydrophobic one, demands more roughness. Now, two approaches are generally adopted to achieve the hydrophobic property of the MLA.[20,21] One is to prepare a micron or nanonipple array directly on the surface of the microlenses, which can improve the hydrophobic performance while bringing a great impact on the imaging performance, transmittance, and other optical properties. The other one is to add some bionic structures, such as columns and cylinders, in the gap between the microlenses,[22−28] which can maintain the optical behavior while improving the hydrophobic performance. However, in order to prepare the structures with different property, multiple micron or nano fabrication methods are often adopted to prepare the superhydrophobic MLA. Recently, Li et al.[23] realized the superhydrophobic MLA structure based on the fabrication integrating three technologies of photolithography, micron-nano printing, and chemical growth. According to the method, the photolithographic mask plate is indispensable, and an extremely high alignment accuracy is needed between the microlens and the hydrophobic structure. The higher alignment accuracy demands the larger gap between the microlens and the hydrophobic structure,[20,22,23,28] which will make the structural performance
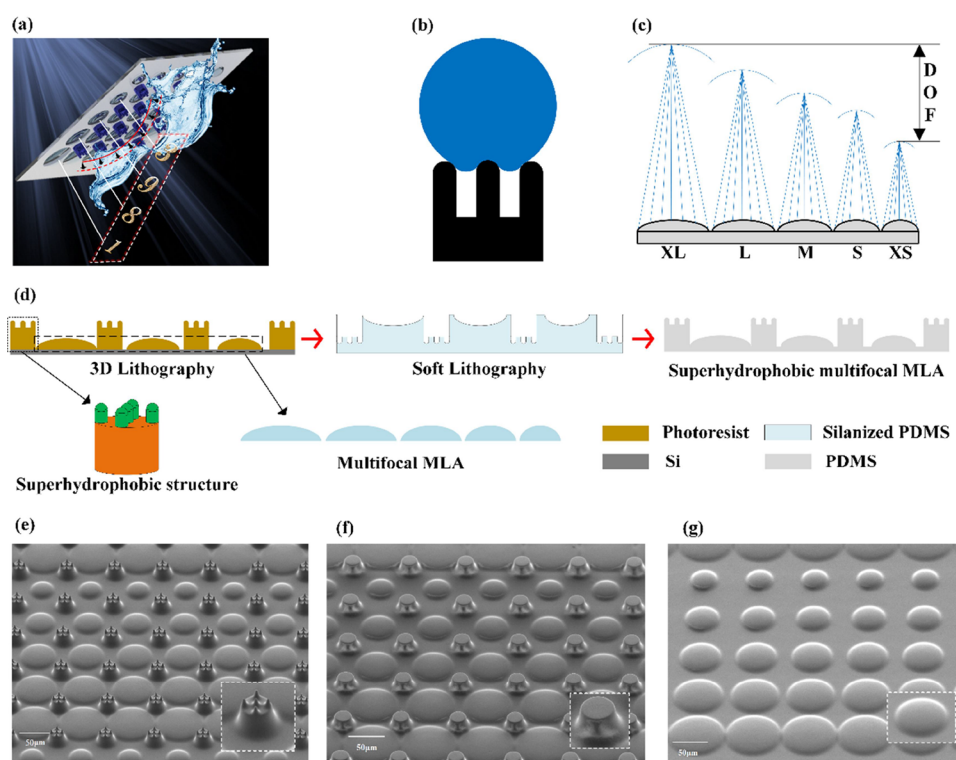
Figure 1. Design and preparation. (a) Diagram of superhydrophobic multifocal MLA functions. (b) Diagram of superhydrophobic principles. (c) Diagram of multifocal function principles. (d) Diagram of the preparation process. (e–g) SEM photos of the microlenses.

greatly impacted, the surface space failed to be fully utilized, and the design to be greatly restricted. In addition, the complex process will result in a limit on material selection, low efficiency, and a failed preparation on a large scale.[29]

To realize the multifocal property of MLA, researchers have carried out a lot of studies and they usually adopt additional driving forces, such as electromagnetic force, photothermal driving force, pressure, and so on.[30–35] However, the need of power source results in more processes and less efficiency, which greatly increases the difficulty of fabrication; moreover, the excessive size will also make the applications greatly restricted.[36–41] How can we achieve superior physical performance both in optics and in superhydrophobic by using micro/nanostructure is still a significant challenge in the related fields.

First of all, due to the high design and preparation freedom of 3D lithography, a multifocal MLA with varying apertures and a multistep superhydrophobic structure with a round dome are designed and molded in a one-piece manner through 3D lithography with no mask. The high preparation freedom of 3D lithography will significantly reduce the complexity of the manufacturing process and improve the design freedom and better optimize the structural parameters for achieving better performance. Then, the multifocal MLA with superhydrophobic properties is successfully transferred to polydimethylsiloxane (PDMS) by means of soft lithography. The MLA with a base diameter in the range of 50–120 μm exhibits excellent superhydrophobic performance. The water droplet can slide at a rolling angle of less than 12.9° and bounce off the surface; meanwhile, with five different focal planes, the detection range can reach 397 μm to sense the surrounding objects so as to get more complete and clearer images by recognizing and compiling a large amount of information collected; in humid environments, the superhydrophobic multifocal MLA can maintain perfect superhydrophobic performance and optical property, which fully display its great potential for application in humid environments as well as broad prospects in biomedical fields.

2. RESULTS AND DISCUSSION

2.1. Design and Fabrication. The microstructure for superhydrophobic and for multifocal length is combined together, as shown in Figure 1a. Figure 1b shows that the superhydrophobic structure adopts a cylindrical frame and a curved protrusion on the top of the cylinder, which can help the water droplets slide down. As shown in Figure 1c, the microlenses with different focal lengths are adopted to form the MLA so that it has continuously multifocal imagine function to detect the DOF of the surrounding objects.

Figure 1d shows the fabrication process of superhydrophobic multifocal MLA. First of all, the designed superhydrophobic structures and multifocal MLA are prepared on the photoresist in one go through 3D lithography; then, the first soft lithography is performed to transfer the pattern structure on the photoresist plate to the PDMS soft template through the pattern transfer technology; finally, the multifocal MLA and superhydrophobic microstructures are transferred onto the PDMS through a soft template to prepare the superhydrophobic multifocal MLA. Figure 1e–g shows the SEM photos with different types of MLA. The preparation method in this paper has the advantages as follows: (1) without other processes and steps or lithography alignment being needed, the 3D lithography can prepare the MLA with different focal lengths and the superhydrophobic microstructures with higher depth-to-width ratio in one go, which shows high level freedom in design and fabrication as well as
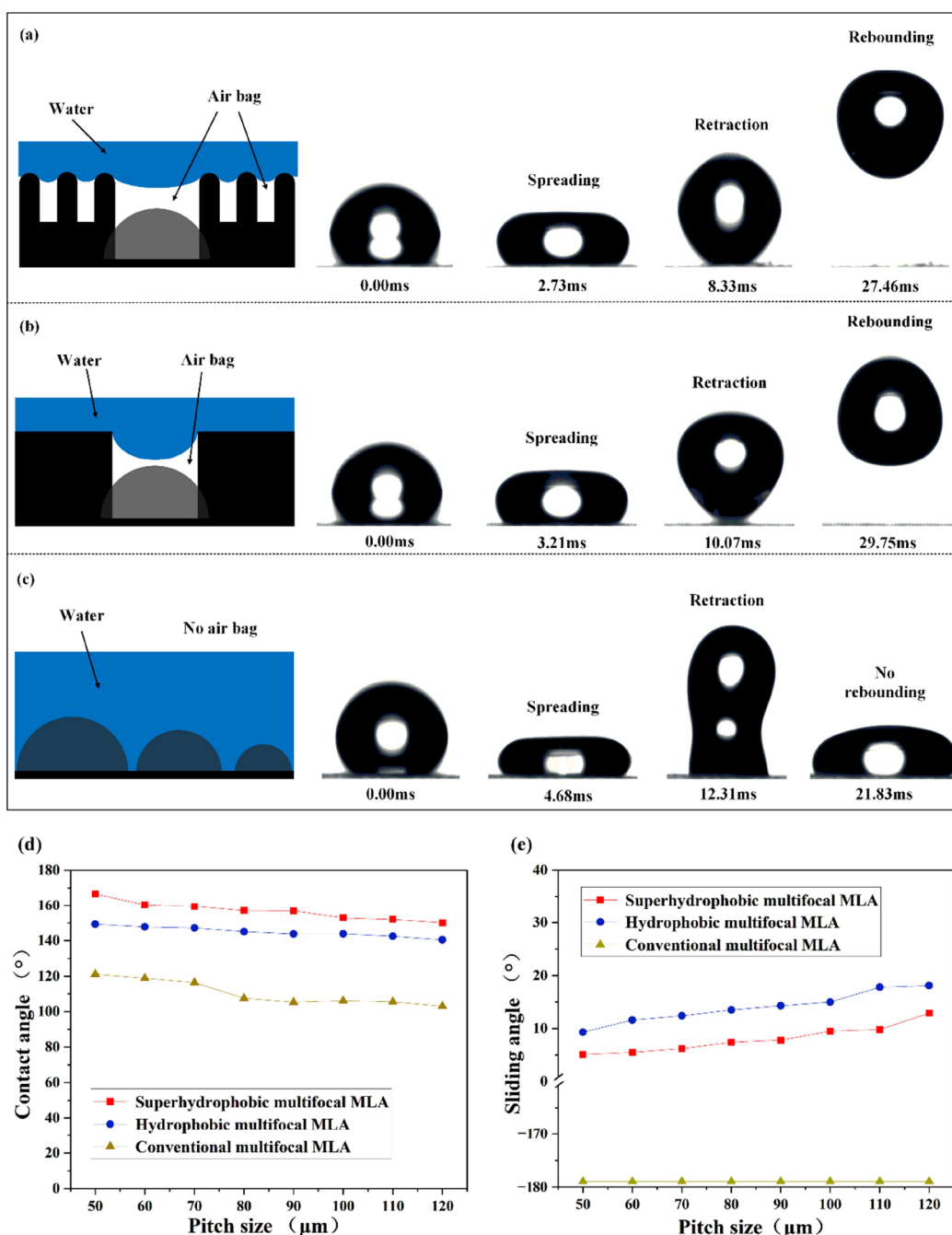
Figure 2. Hydrophobicity test and analysis: (a−c) dynamic performance of different types of MLAs; (d) contact angle of different types of MLAs; and (e) sliding angle of different types of MLAs.

relatively simple process. (2) The preparation of superhydrophobic microstructures and the processing of microlenses with low surface roughness were completed simultaneously. Since 4096 gray steps can be designed on the *z*-axis, the surface roughness of different regions on the structure surface can be adjusted arbitrarily so as to process the surfaces with different properties in one go. (3) PDMS with excellent mechanical properties and thermal stability are selected as soft templates, which have been widely applied in multiple fields such as materials, biology, and microfluid. The processing efficiency of up to 280 mm²/min can be realized based on the 3D lithography. The preparation method introduced in this paper indicates the possibility of fabricating superhydrophobic

multifocal MLA in a large-scale, low-cost, and high-efficiency manner.

2.2. Hydrophobicity. Figure 2a−c demonstrates the dynamic performance of water droplets (4 μL) falling on different types of MLA. The first column shows the diagram of a superhydrophobic multifocal MLA, a hydrophobic multifocal MLA and a conventional multifocal MLA when water droplet is attached to the surface under the condition of 80 μm cycle size. The 2−5 columns show the dynamic performance analysis when water drop falls on the surface, and the experimental result is as follows: when the water droplet falls on the superhydrophobic multifocal MAL (as shown in the water droplet dropping on superhydrophobic multifocal MLA of Supporting Information), it spreads to the maximum area and

then starts to shrink at 2.73 ms, the droplet shrinks to the minimum volume and starts to rebound at 8.33 ms, and the rebound reaches the highest point at 27.46 ms; when the water droplet falls on the hydrophobic multifocal MLA (as shown in the water droplet dropping on hydrophobic multifocal MLA of Supporting Information), it starts to shrink after spreading for 3.21 ms and starts to rebound after shrinking for 10.07 ms, and the rebound reaches the highest point at 29.75 ms; when the water droplet falls on a conventional multifocal MLA (as shown in the water droplet dropping on multifocal MLA of Supporting Information), the spreading time lasts for 4.68 ms while the spreading area is larger and the height is lower compared to the aforesaid two types of MLAs, then it starts to shrink at 12.31 ms and the water droplet spreads once again to the maximum radius at 21.83 ms instead of rebounding.

Superhydrophobic multifocal MLA has the shortest spread time, the shortest contact time between the droplet and the surface, and the shortest time to rebound to the highest point. Since the small cylinder increases the height of gas−liquid interface and reduces the contact area of solid−liquid interface, it enables the whole structure to have a larger volume of "airbag", as shown in the first column of Figure 2a−c, the larger volume of "airbag" makes the droplet hard to contact the microlens, which can reduce the spreading of droplet and make it quickly shrink and rebound after reaching the lowest point. In addition, a semicircular arc is designed at the top of the cylinder to help the droplet contact the structure more smoothly when it falls on the surface with better protection from being punctured. In the process of droplet spreading, the semicircular arc on the top can realize better contact and integrate with the droplets and delay the droplet spreading. In the process of droplet shrinking, the droplet can escape from the semicircular arc on the top more quickly to realize quick shrinking and rebounding. In contrast, the hydrophobic multifocal MLA has a slightly longer spread time, longer contact time between the droplet and the surface, and longer time to rebound to the highest point. Since there is no small cylinder in the hydrophobic structure compared to the superhydrophobic one, the height of the gas−liquid interface is lower and the contact area of the solid−liquid interface is also larger than that of the superhydrophobic one. Therefore, it is even harder for the droplet to escape from the surface due to high spread depth and longer contraction process. In addition, the top of the cylinder is not designed as the shape of a semicircular arc; the edges are so sharp that the droplet is more likely to be deformed when it contacts with the surface, which makes the whole process more complicated and time-consuming. As for the traditional multifocal MLA, the droplet covers the whole surface without "airbag" between the droplet and the microstructure, which leads to the deepest droplet spreading with longest time, so the droplet cannot escape from the surface of the traditional multifocal MLA after shrinking.

Usually, a method of surface micron-nano structure and chemical modification is adopted to prepare the superhydrophobic surface. The performance of superhydrophobic multifocal MLA proposed in this paper can be realized directly by microstructures without any chemical post-treatment on the surface. For different applications, the microlenses with different aperture need to be designed and prepared, so the gap of superhydrophobic structures composited between microlenses of various apertures may also change, resulting in an impact on the hydrophobicity. Therefore, it is necessary to study the impact of the structure gap on the hydrophobicity

to provide a reference for the performance optimization of the structures at the same time. As shown in Figure 2d−e, three different types of multifocal MLA with structural periods of 50, 60, 70, 80, 90, 100, 110, and 120 μm are prepared with the measurement of the contact angles and sliding angles. The droplet rebounding times and contact times of different types of multifocal MLA with different periods also were measured as shown in Figures S1 and S2 of the Supporting Information.

Figure 2d shows the results of the measured contact angle, and it can be found that the contact angles of superhydrophobic multifocal MLA with period sizes of 50, 60, 70, 80, 90, 100, 110, and 120 μm are all higher than 150° with excellent superhydrophobic performance, which verifies that the small cylindrical structure and the semicircular arc on the top can enhance the surface hydrophobicity. As the period increases, the contact angle decreases. We can explain this phenomenon with Cassie−Baxter theory[42−44] as the following description:

$$\cos \theta = r_\mathrm{f} \cos \theta_\mathrm{y} + f - 1$$

θ is the apparent contact angle in the Cassie−Baxter state, θ_y is the contact angle of the ideal surface without microstructure, f is the contact area of the prepared solid surface with the water droplet, and r_f is the ratio of the actual area of the surface to the projected area. The second-order roughness columns can prevent water droplets from contacting the surface to form the Cassie−Baxter state at the interface. The more second-order roughness columns per unit area, the better are the hydrophobic properties. The hydrophobic multifocal MLA with the same period has a maximum contact angle of 149.3° at a period structure of 50 μm, and the contact angle decreases while the period increases, which is also the reason for increasing the gap as the period increases. It can be discovered that the superhydrophobic multifocal MLA with small cylinders and top semicircular protrusions on the hydrophobic structure has a larger contact angle compared to the hydrophobic multifocal MLA without similar structures. This can be explained by the fact that the small cylindrical structure and the semicircular protrusion at the top increase the area of the surface at the upper end, thus increasing the height of the gas−liquid interface between the water droplet and the air. The higher gas−liquid interface height results in a smaller contact area of the water droplets with the structure and a smaller contact area at the solid−liquid interface, which helps increase the contact angle. The conventional multifocal MLA of the same cycle has no hydrophobic structure, and water droplets will directly cover the structure surface, resulting in a smaller contact angle when the droplets are in the Wenzel state. The experimental results show that the contact angle of the multifocal MLA with hydrophobic structure will be significantly enhanced due to the presence of hydrophobic structures compared to the conventional multifocal MLA without the composite hydrophobic structures, especially for the superhydrophobic multifocal MLA, whose design of small cylinders and the top semicircular arc protrusions on the superhydrophobic structures can enhance the hydrophobicity of multifocal MLA to the superhydrophobic performance.

As shown in Figure 2e, this refers to the roll angle measurement of the aforementioned structure. It can be discovered that the conventional multifocal MLA, which has no hydrophobic structure on the surface, does not allow water droplets on the surface to roll or escape the surface of the multifocal MLA. When the hydrophobic structures are
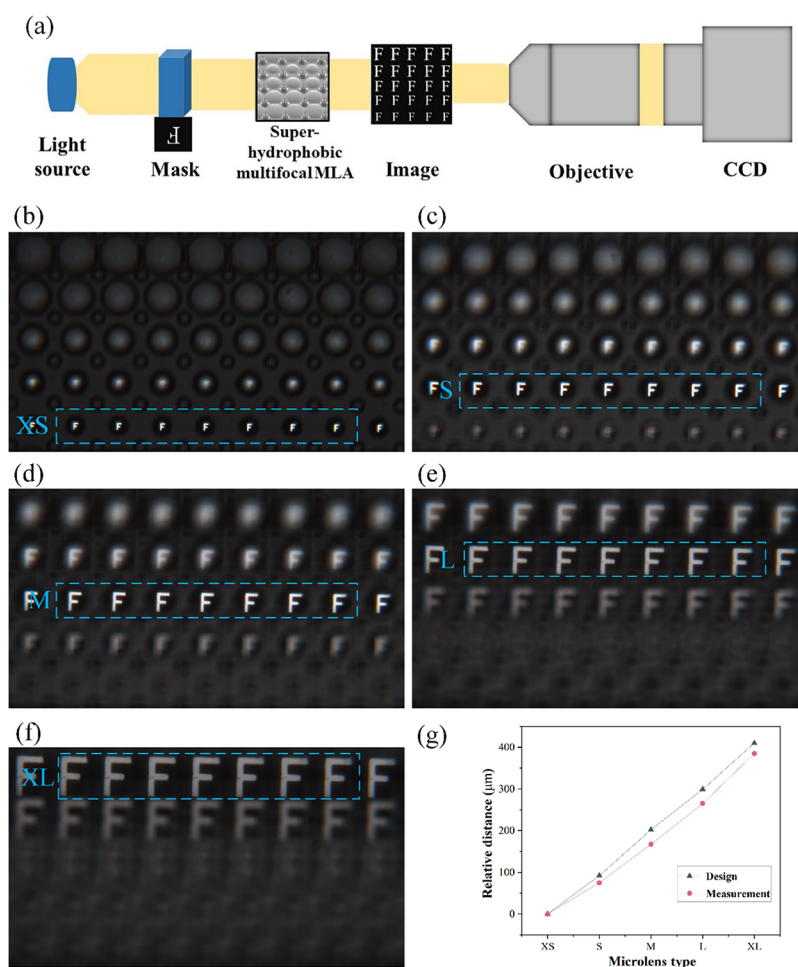
Figure 3. Multifocal imaging performance test: (a) refers to the experimental setup to test the imaging performance; (b) refers to the XS microlens imaging; (c) refers to the S microlens imaging; (d) refers to the M microlens imaging; (e) refers to the L microlens imaging; (f) refers to the XL microlens imaging; and (g) refers to the relative distances between the images of different types of microlenses and the corresponding objects.

compositely prepared between multifocal MLA, the water droplets on the surface can roll on or escape from the surface, and the rolling angle becomes larger while the period increases. It is due to the presence of hydrophobic structures that increase the height of the gas−liquid interface and reduce the resistance against the droplets on the surface, thus enabling them to roll off. When the period becomes larger, the gap between the structures and the resistance against the droplets to roll off will also become larger, so that a larger tilting angle is needed for the droplets to roll off. When the superhydrophobic structures are compositely prepared between multifocal MLA, the water droplets on a surface can roll on or off its surface more easily. It is due to the fact that the small cylinders on the superhydrophobic structure can further raise the height of the gas−liquid interface and the top semicircular arc can achieve a smoother contact with the droplets, which will greatly reduce the resistance against the droplets to roll, and thus the droplets on the superhydrophobic MLA are much easier to roll on or off.

2.3. Performance of Multifocal Imaging. In real life, the objects to be observed are often in different focal planes, so mammals have to adjust the curvature of their eyes to change the focal length to see objects clearly in different focal planes, and this multifocal imaging function helps them with the ability to perceive the depth of field. Similarly in this paper, the microlenses with five focal lengths are prepared within the gap

of superhydrophobic microstructures and combined into arrays, to have the function of multifocal imaging and depth-of-field perception.

Figure 3a shows the optical device to test the imaging performance of superhydrophobic multifocal MLA, in which the asymmetric pattern mask "F" is selected as the object of research. The "F" mask is placed between the superhydrophobic multifocal MLA and the white light source, the objective lens and the CCD are placed behind the superhydrophobic multifocal MAL sequentially. All devices are maintained in the same axial height. When the light source is turned on, the image of the "F" mask is observed and received by the observation system consisting of the objective lens and the CCD.

Figure 3b−f shows the optical images formed by different types of microlenses in the superhydrophobic multifocal MLA at different relative distances, and these images are captured by the 10× objective lens and the CCD set behind. The multifocal imaging capability is described by the relative distances between the superhydrophobic multifocal MLA and the "F" mask in this paper. According to Figure 3b, a clear "F" image can be observed from the XS-type microlens in the superhydrophobic multifocal MLA, and now the relative distance from the "F" mask is set as 0 μm. In Figure 3c, when the relative distance is enlarged, the clear "F" image can be seen from the S-type microlens. It can be seen that the
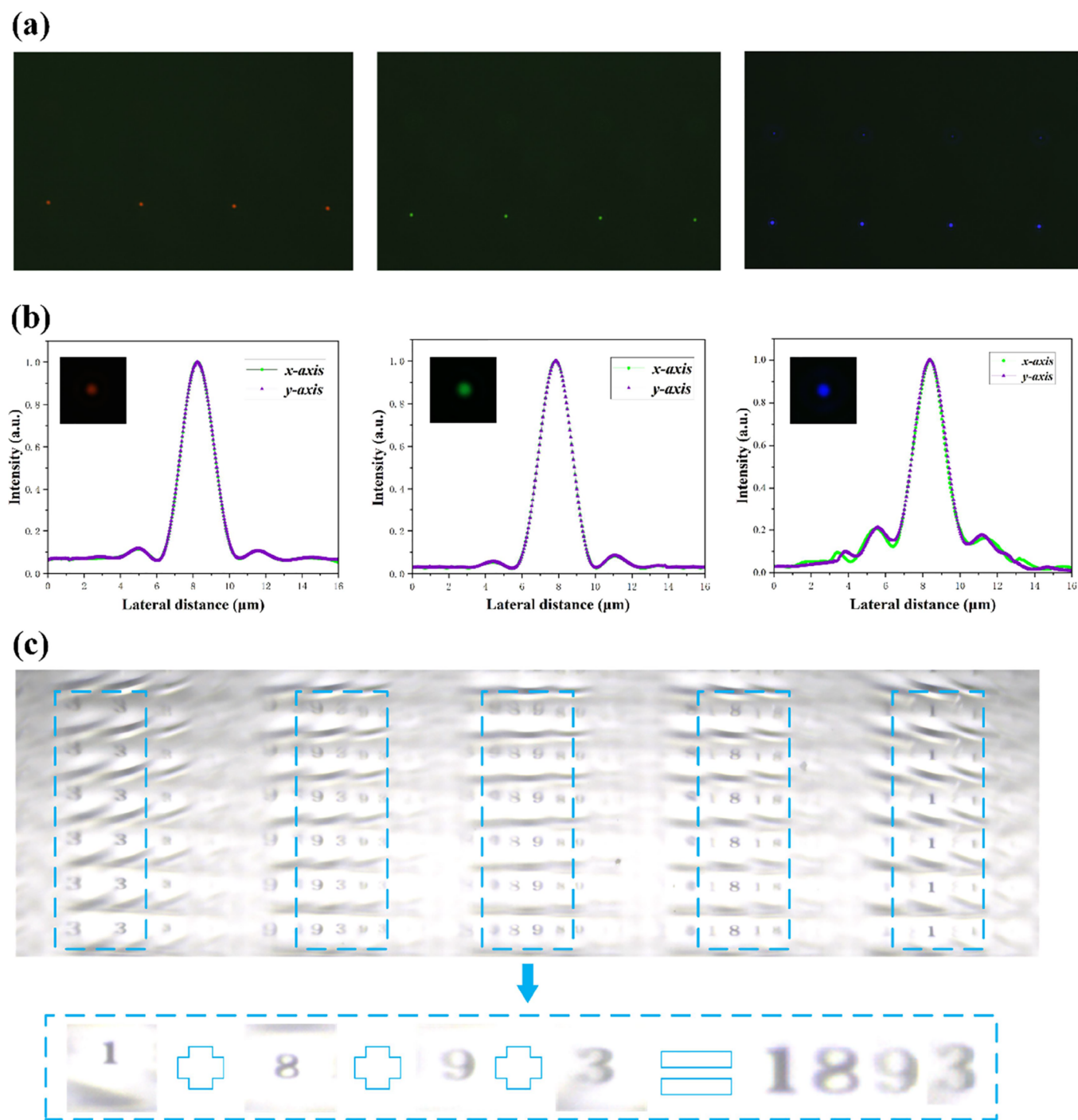
Figure 4. Optical performance test: (a) refers to a plot of spot convergence under different wavelengths of laser; (b) refers to a comparison of intensity distribution of converged focus under laser irradiation of different wavelengths (along the *x*-axis and *y*-axis); and (c) refers to the process of information sharing and compilation.

image size of the S-type microlens is larger than that of the XS-type microlens, because the position of the S-type microlens is higher than that of the XS-type microlens while the objective distance of the S-type microlens is larger than that of the XS-type microlens; therefore, the image by the S-type microlens is larger than that by the XS-type microlens. As shown in Figure 3d−f, continue to rotate the button to expand the relative distance. As the relative distance increases, the clear "F" image by the XS-type and S-type microlenses will gradually shift to the M-type and L-type microlenses and then finally move to the XL-type microlens at a relative distance of 397 μm, while

the image has never been distorted during the process. This imaging ability at different focal planes may enable the superhydrophobic multifocal MLA with multifocal imaging function so as to perceive the DOF of the surrounding objects (as shown in the multifocal imaging of superhydrophobic multifocal MLA of Supporting Information)

Figure 3g shows the relative distances at which different types of microlenses are imaged. As the image is shifted from XS to XL and the relative distance increases from 0 to 397 μm, the experimental values of relative shift distance in the test are close to the design values, and the relative shift distance varies
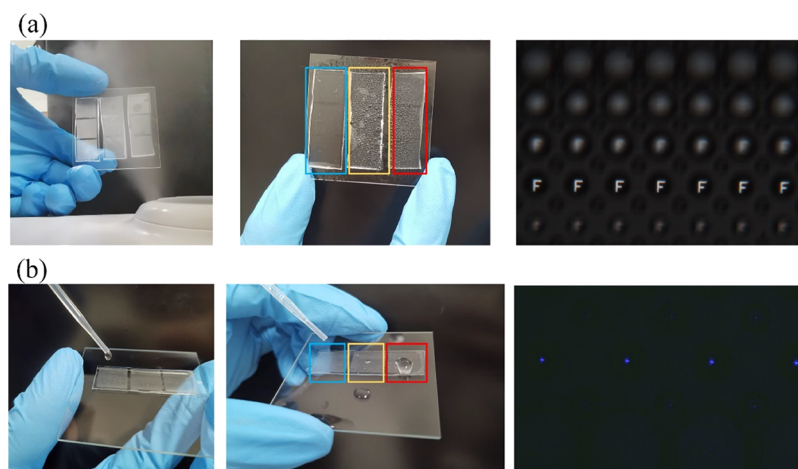
Figure 5. Experiments in different environments. (a) Optical imaging after simulated rain shower. (b) Spot convergence in a simulated high-humidity environment.

almost in a linear manner, which makes the depth of field easy to be estimated. However, the experimental values are relatively small because of the deformation of PDMS adhesive during the structure transfer. The PDMS adhesive will undergo thermal curing deformation once being heated, and the final microlens may not be in a perfect aspheric shape; thus, some performance may be affected. In addition, the superhydrophobic multifocal MLA has perfect imaging performance at five imaging distances, which makes no difference with that of the conventional multifocal MLA without the superhydrophobic structures on the surface. It means that the superhydrophobic structure has no influence on the imaging performance of the multifocal MLA.

2.4. Optical Performance of the Fabricated AMLAs. Focal ability, which is often used by many researchers to evaluate the optical performance of MLA, is an important feature of many optical devices. As shown in Figure 4a, the spot convergence function of superhydrophobic multifocal MLA is tested when irradiated by lasers at wavelengths of 450, 520, and 635 nm respectively, and the images are shot by a 20X objective lens and a CCD. The experimental results show that the superhydrophobic multifocal MLA is capable of beam convergence very well.

Figure 4 shows the intensity distribution of focal light intensity along the x-axis and y-axis after normalization. According to the experimental results, as for the aforesaid wavelengths, the light intensity distribution of the focal point along the x-axis and y-axis is in good agreement, and the half-width of the focal point is less than 2 μm with very good convergence performance. According to the intensity distribution of the focal point, there are some ring halos or multilevel diffractions around the focal point, which may result from the surface roughness; however, the intensity of the ring halo is much lower than that of the secondary diffraction resulting from the plane diffractive MLA. The aspherical MLA with good focal intensity distribution is highly sensitive to laser wavelength, so it can be applied to a variety of new micro-optical sensor devices.

By changing the relative distance between the superhydrophobic multifocal MLA and the objective lens, different types of microlenses show the phenomenon of spotted focus sequentially. It indicates that the superhydrophobic multifocal MLA mentioned in this paper is capable of information sharing

and multifocal imaging, which means that a large amount of information can be collected from more areas for identification and compilation. Figure 4c shows the process of information collection and compilation. Place the number "1893" (the birth year of Wuhan University) between the light source and the superhydrophobic multifocal MLA, and we can get different images with different types of microlenses. On some images, the numbers "1" or "3" are alone, while on some the numbers "93", "89" and "18" are converged together. Compared to conventional MLA, it can capture object information in a more comprehensive manner. When the captured images are recognized and compiled, it can be seen that the number "1" is to the left of the number "8", and the number "3" is to the right of the number "9". After determining the location of all the images, the clearest image is selected for editing and compiling so that a clearer and more complete image "1893" can be obtained, as shown at the bottom of Figure 4c.

2.5. Optical Imaging Properties in a Humid Environment. In this paper, the flexible material PDMS is used to prepare the superhydrophobic multifocal MLA. Since the material for preparation is flexible, it can be applied to the field of flexible display electronic devices. The optical properties of different samples are tested under water droplet impact, friction (as shown in Figure S4 of the Supporting Information), and high-humidity environment to verify the adaptability in different environments. The superhydrophobic multifocal MLA, the hydrophobic multifocal MLA and the conventional multifocal MLA are marked with the blue, yellow, and red frames, respectively.

Figure 5a shows the adaptation experiment in a high-humidity environment, in which different types of microlenses are placed near a humidifier to simulate the humid outdoor environments such as early morning, foggy day, and waterside. Different types of samples with clean surfaces are placed on top of the humidifier, and then power on the humidifier to make the humidity of the experimental environment approach 100%, and then keep the samples on top of the humidifier for 5 min for observation. According to the experimental results, the vapor condenses into droplets on the surface of the samples, and the condensed droplets on the superhydrophobic multifocal MLA can roll off without residue; however, there are some residual droplets on the surface of the hydrophobic multifocal MLA and a large number of droplets condensed on

the conventional multifocal MLA. The optical imaging performance of three MLA in a high-humidity environment has been tested. Since there are no water droplets adhered to the surface, the image by the superhydrophobic multifocal MLA is clear and complete with high imaging quality, whereas the imaging quality of the hydrophobic multifocal MLA is degraded due to the influence of the water droplets, and the conventional multifocal MLA is hardly capable of imaging due to the excessive water droplets on the surface.

As shown in Figure 5b, when the water droplets are dropped on different MLAs, it can be seen that different samples will show different performances. The water droplets will not adhere to the superhydrophobic multifocal MLA at all; some water droplets will adhere to the hydrophobic multifocal MLA and the water droplets will completely adhere to the conventional multifocal MLA, which can fully verify the correctness of our structural design. In the case of water droplets on the surface, the beam focusing performance of the three MLAs has been tested. Since there are no water droplets adhered to the surface, the superhydrophobic multifocal MLA converges to a clear and bright light spot, while the beam convergence performance of the hydrophobic multifocal MLA and the conventional multifocal MLA is relatively poor.

According to the aforesaid experiments, the structure illustrated in this paper can successfully integrate the superhydrophobic and multifocal imaging functions under the environments of near 100% humidity, rain, and mild abrasion, so it has a broad prospective application in the future. However, if the size of the water droplet is smaller than the gap of the superhydrophobic structure or the structure has been worn out, it is necessary to design the superhydrophobic structure with a smaller gap and more robust materials to avoid the structural damages.

3. CONCLUSIONS

Conclusively speaking, the method of combining 3D lithography with soft lithography can be adopted to prepare the superhydrophobic multifocal MLA with superhydrophobic properties and a multifocal imaging function in a simple and efficient manner. The superhydrophobic multifocal MLA has good superhydrophobic performance at the gap of 50−120 μm. Water droplets can roll off the surface at a rolling angle of less than 12.9° and bounce off the surface. Apart from the superhydrophobic performance, it is capable of multifocal imaging and integrated imaging with a DOF detection range of up to 397 μm. In addition, it can maintain good superhydrophobic performance and optical properties in an extremely humid environment. The superhydrophobic multifocal MLA proposed in this paper has a broad perspective on the actual applications.

4. EXPERIMENTAL SECTION

The main fabrication process of the h-MLA includes two steps: a 3D lithography process and a PDMS replication process.

4.1. 3D Lithography Process. A PR (Merck, AZ4562) was spin-coated on a Si substrate with a thickness of 1 mm. It was spin-coated at a speed of 550 rpm for 35 s and relaxed for 30 min. Subsequently, 3D lithography technology (4PICO, Pico Master 100) was directly used to perform grayscale exposure of the PR. The exposure dose was 1200 mJ/mm². The working laser wavelength was 850 nm. The working speed of the laser spot was 100 mm/s. At a ratio of 3:1 (by weight),

ultrapure water was mixed with the developer (AZ 400 K). The development time was 10 min. The acquired MLA was baked for 20 s at 90 °C.

4.2. PDMS Replication Process. A PDMS elastomer kit (Sylgard 184) was purchased from Dow Corning (MI). At a ratio of 10:1 (by weight), the PDMS prepolymer was mixed with the cross-linker and degassed for 15 min at 50 °C. The mixture was poured onto the PR, followed by curing at 80 °C for 3 h. After peeling off the PDMS mixture from the PR, a negative mold was acquired and placed on glass. Then, the PDMS mold was coated with 1H, 1H, 2H, 2H perfluorodecyltriethoxysilane after plasma treatment with an oxygen ion. The PDMS mold coated with 1H, 1H, 2H, 2H perfluorodecyltriethoxysilane was placed in a vacuum environment for 40 min and was coated with the PDMS mixture again. Next, the silanized negative mold was spin-coated with 1 mm thick PDMS, and a second hot-curing process was employed on the negative mold to realize pattern replication. The negative mold with PDMS was placed in an oven again at 80 °C for 3 h to realize curing. After the PDMS film was peeled off of the negative mold, the fabrication of the MLAs was completed.

4.3. Characterization. SEM images of the gold-sputtered samples were taken with a field-emission scanning electron microscope (Tescan, Brno, s.r.o.). The transmittance of the samples was measured with a UV spectrophotometer (Lambda 365 UV−vis spectrophotometer, PerkinElmer). The components of the optical measurement system included an objective lens (Daheng, GCO-2107), two light sources (Thorlab, CPS635; Lemons, KMFL2929), and a charge-coupled device (CCD) (Daheng, MER-2000-19U3C-L).

■ ASSOCIATED CONTENT

Ⓢ Supporting Information

The Supporting Information is available free of charge at https://pubs.acs.org/doi/10.1021/acsomega.3c08680.

> Water droplet dropping on a superhydrophobic multifocal MLA (AVI)
>
> Water droplet dropping on a hydrophobic multifocal MLA (AVI)
>
> Water droplet dropping on a multifocal MLA (AVI)
>
> Multifocal imaging of a superhydrophobic multifocal MLA (MP4)
>
> Rebounding times of different types of MLAs; contact time between the liquid droplet and different types of MLAs; transmittance result; and imaging results of a conventional MLA (PDF)

■ AUTHOR INFORMATION

Corresponding Authors

Su Shen − *School of Optoelectronic Science and Engineering, Collaborative Innovation Center of Suzhou Nano Science and Technology, Soochow University, Suzhou 215006, China;* Email: sushen@suda.edu.cn

Chengqun Gui − *The Institute of Technological Sciences, Wuhan University, Wuhan 430072, China;* Email: cheng.gui@whu.edu.cn

Authors

Hao Cao − *The Institute of Technological Sciences, Wuhan University, Wuhan 430072, China;* ⓘ orcid.org/0000-0003-0560-7226

Hongfeng Deng − *The Institute of Technological Sciences, Wuhan University, Wuhan 430072, China;* orcid.org/0000-0003-3201-1081

Hui Wan − *School of Power and Mechanical Engineering, Hubei Key Laboratory of Electronic Manufacturing and Packaging Integration, Wuhan University, Wuhan 430072, China*

Shiyi Luan − *The Institute of Technological Sciences, Wuhan University, Wuhan 430072, China;* orcid.org/0000-0001-6334-6058

Complete contact information is available at:
https://pubs.acs.org/10.1021/acsomega.3c08680

Notes
The authors declare no competing financial interest.

■ REFERENCES

(1) Jiang, P.; McFarland, M. J. Wafer-Scale Periodic Nanohole Arrays Templated from Two-Dimensional Nonclose-Packed Colloidal Crystals. *J. Am. Chem. Soc.* **2005**, *127*, 3710−3711.

(2) Sohn, I.-B.; Choi, H.-K.; Noh, Y.-C.; Kim, J.; Ahsan, M. S. Laser Assisted Fabrication of Micro-Lens Array and Characterization of their Beam Shaping Property. *Appl. Surf. Sci.* **2019**, *479*, 375−385.

(3) Cheng, Y.-C.; Chen, C.-C.; Hsu, W.-Y.; Wang, P. J.; Tsai, D. P. The Fabrication of High Filling Factor Double Side Micro Lens Array with High Alignment Accuracy. In *SPIE Optical Engineering Applications, Optical Manufacturing and Testing IX*; SPIE: San Diego, United States, 27 September, 2011.

(4) Lin, V.; Wei, H.-C.; Hsieh, H.-T.; Su, G.-D. J. An Optical Wavefront Sensor Based on a Double Layer Microlens Array. *Sensors* **2011**, *11*, 10293−10307.

(5) Kumar, M. S.; Sharma, R.; Narayanamurthy, C. S.; Kumar, A. S. K. Determination of the Focal Length of Microlens Array by Spherical Wavefronts. *Opt. Eng.* **2014**, *53*, No. 064102.

(6) Yu, X.-H.; Wang, Z.; Han, Y.-C. Microlenses Fabricated by Discontinuous Dewetting and Soft Lithography. *Microelectron. Eng.* **2008**, *85*, 1878−1881.

(7) Chen, S. H.; Yi, X. J.; Li, Y.; He, M.; Chen, S. X.; Kong, L. B. Design of Diffractive Microlens Array Integration with Focal Plane Arrays. In *Optics and Optoelectronic Inspection and Control: Techniques, Applications, and Instruments, Biomedical Photonics and Optoelectronic Imaging*; SPIE: Beijing, China, 5 November, 2000.

(8) Pang, Y. F.; Xu, C. T.; Cao, A.; Shi, L. F.; Fu, Y.; Pang, Hu.; Deng, Q. L.; Liu, L. W.; Liu, W. J. Light Field Acquisition using Microlens based on 3ds Max and Image Reconstruction Technology, SPIE/COS Photonics Asia. In *Advanced Optical Imaging Technologies*; SPIE, 2018.

(9) Colonnier, F.; Manecy, A.; Juston, R.; Viollet, S. Visual Odometry and Low Optic Flow Measurement by Means of a Vibrating Artificial Compound Eye. In *Conference on Biomimetic and Biohybrid Systems 4th International Conference, Living Machines*, Barcelona, Spain, July 28−31, 2015.

(10) Li, J.; Wang, W.; Mei, X.; Hou, D.; Pan, A.; Liu, B.; Cui, J. Fabrication of Artificial Compound Eye with Controllable Field of View and Improved Imaging. *ACS Appl. Mater. Interfaces* **2020**, *12*, 8870−8878.

(11) Yuan, S.; Yin, J.; Jin, J.; Song, L.; Ma, J.; Yan, S.; Luan, S. Facile fabrication of Microsphere-polymer Brush Hierarchically Threedimensional (3D) Substrates for Immunoassays. *Chem. Commun.* **2015**, *51*, 6749−6752.

(12) McIntire, J. P.; Havig, P. R.; Geiselman, E. E. Stereoscopic 3D displays and Human Performance: A Comprehensive Review. *Displays* **2014**, *35*, 18−26.

(13) Muthe, L. P.; Pickering, P. K.; Gauss, C. A Review of 3D/4D Printing of Poly-Lactic Acid Composites with Bio-Derived Reinforcements. *Compos., Part C: Open Access* **2022**, *8*, No. 100271.

(14) Zhu, Y. Z.; Tang, T. T.; Zhao, S. Y.; Joralmon, D.; Poit, Z.; Ahire, B.; Keshav, S.; Raje, A. R.; Blair, J.; Zhang, Z. L.; Li, X. J. Recent Advancements and Applications in 3D printing of Functional Optics. *Addit. Manuf.* **2022**, *52*, No. 102682.

(15) Ratcliff, J.; Supikov, A.; Alfaro, S.; Azuma, R. ThinVR: Heterogeneous Microlens Arrays for Compact, 180 degree FOV VR Near-eye Displays. *IEEE Trans. Visual. Comput. Graph.* **2020**, *26*, 1981−1990.

(16) Darkhanbaatar, N.; Erdenebat, M.-U.; Shin, C.-W.; Kwon, K.-C.; Lee, K.-Y.; Baasantseren, G.; Kim, N. Three-dimensional Aeethrough Augmented-reality Display System using a Holographic Micromirror Array. *Appl. Opt.* **2021**, *60*, 7545−7551.

(17) Neinhuis, C.; Barthlott, W. Characterization and Barthlott, W. Characterization and Distribution of Water-repellent, Self-cleaning Plant Surfaces. *Ann. Bot.* **1997**, *79*, 667−677.

(18) Pahlevaninezhad, H.; Khorasaninejad, M.; Huang, Y. W.; Shi, Z.; Hariri, L.; Adams, D.; Ding, V.; Zhu, A.; Qiu, C.; Capasso, F.; Suter, M. Nano-optic endoscope for high-resolution optical coherence tomography in vivo. *Nat. Photonics* **2018**, *12*, 540−547.

(19) Zhou, Y.; Xiong, B. O.; Song, W.; Zhang, X. U.; Zheng, G.; Dai, Q.; Cao, X. Light-field micro-endoscopy using a fiber bundle:a snapshot 3d epi-fluorescence endoscope. *Photonics. Research.* **2022**, *10*, 2247−2260.

(20) Zheng, L.; Zhang, Y.; Lin, H.; Kang, S.; Li, Y.; Sun, D.; Chen, M.; Wang, Z.; Jiao, Z.; Wang, Y.; Dai, B.; Zhuang, S.; Zhang, D. Ultrasound and Near-Infrared Light Dual-Triggered Upconversion Zeolite-Based Nanocomposite for Hyperthermia-Enhanced Multimodal Melanoma Therapy via a Precise Apoptotic Mechanism. *ACS Appl. Mater. Interfaces* **2020**, *12*, 32420−32431.

(21) Yong, J.; Bian, H.; Yang, Q.; Hou, X.; Chen, F. Mini-Review on Bioinspired Superwetting Microlens Array and Compound Eye. *Front. Chem.* **2020**, *8*, No. 575786.

(22) Li, M.; Yang, Q.; Chen, F.; Yong, J.; Bian, H.; Wei, Y.; Fang, Y.; Hou, X. Integration of Great Water Repellence and Imaging Performance on a Superhydrophobic PDMS Microlens Array by Femtosecond Laser Microfabrication. *Adv. Eng. Mater.* **2019**, *21*, No. 1800994.

(23) Li, J.; Wang, W.; Mei, X.; Pan, A. Designable Ultratransparent and Superhydrophobic Surface of Embedded Artificial Compound Eye with Extremely Low Adhesion. *ACS Appl. Mater. Interfaces* **2020**, *12*, 53557−53567.

(24) Koch, K.; Bhushan, B.; Barthlott, W. Diversity of Structure, Morphology and Wetting of Plant Surfaces. *Soft Matter* **2008**, *4*, 1943−1963.

(25) Koch, K.; Bhushan, B.; Barthlott, W. Multifunctional Surface Structures of Plants: An Inspiration for Biomimetics. *Prog. Mater. Sci.* **2009**, *54*, 137−178.

(26) Sun, T.; Feng, L.; Gao, X.; Jiang, L. Bioinspired Surfaces with Special Wettability. *Acc. Chem. Res.* **2005**, *38*, 644−652.

(27) Dong, Y.; Ma, L.; Tang, C. Y.; Yang, F.; Quan, X.; Jassby, D.; Zaworotko, M. J.; Guiver, M. D. Stable Superhydrophobic CeramicBased Carbon Nanotube Composite Desalination Membranes. *Nano Lett.* **2018**, *18*, 5514−5521.

(28) Wu, D.; Wang, J.-N.; Niu, L.-G.; Zhang, X. L.; Wu, S. Z.; Chen, Q.-D.; Lee, L. P.; Sun, H. B. Bioinspired Fabrication of High-Quality 3D Artificial Compound Eyes by Voxel-Modulation Femtosecond Laser Writing for Distortion-Free Wide-Field-of-View Imaging. *Adv. Opt. Mater.* **2014**, *2*, 751−758.

(29) Liu, F.; Yang, Q.; Chen, F.; Zhang, F.; Bian, H.; Hou, X. Lowcost High Integration IR Polymer Microlens Array. *Opt. Lett.* **2019**, *44*, 1600−1602.

(30) Long, Y.; Song, Z.; Pan, M.; Tao, C.; Hong, R.; Dai, B.; Zhang, D. Fabrication of uniform-aperture multi-focus microlens array by curving microfluid in the microholes with inclined walls. *Opt. Express* **2021**, *29*, 12763−12771.

(31) Lee, J. H.; Chang, S.; Kim, M. S.; Kim, Y. Z.; Kim, H. M.; Song, Y. M. Multifocal Microlens Array through Single-Step Multi-Sized Hole Patterning Photolithography. *Micromachines* **2020**, *11*, 1068.

(32) Miccio, L.; Paturzo, M.; Grilli, S.; Vespini, V.; Ferraro, P. Hemicylindrical and Toroidal Liquid Microlens Formed by Pyro-electro- wetting. *Opt. Lett.* **2009**, *34*, 1075−1077.

(33) Ren, H.; Wu, S.-T. Tunable-focus Liquid Microlens Array Using Dielectrophoretic Effect. *Opt. Express* **2008**, *16*, 2646−2652.

(34) Zhang, W.; Aljasem, K.; Zappe, H.; Seifert, A. Completely Integrated, Thermo-Pneumatically Tunable Microlens. *Opt. Express* **2011**, *19*, 2347−2362.

(35) Cao, J.; Hou, Z.-S.; Tian, Z.-N.; Hua, J.-G.; Zhang, Y.-L.; Chen, Q.-D. Bioinspired Zoom Compound Eyes Enable Variable-Focus Imaging. *ACS Appl. Mater. Interfaces* **2020**, *12*, 10107−10117.

(36) Zhong, Y.; Yu, H.; Zhou, P.; Wen, Y.; Zhao, W.; Zou, W.; Luo, H.; Wang, Y.; Liu, L. In Situ Electrohydrodynamic Jet Printing-Based Fabrication of Tunable Microlens Arrays. *ACS Appl. Mater. Interfaces* **2021**, *13*, 39550−39560.

(37) Jing, X.; Wang, K.; Zhu, R.; Lin, J.; Yu, B.; Lu, M. Design and Fabrication of Double-Layer Curved Compound Eye via Two-Photon Polymerization. *IEEE Photonics Technol. Lett.* **2021**, *33*, 231−234.

(38) Liu, H.; Li, Y.; Lin, W.; Hong, M. High-aspect-ratio crack-free microstructures fabrication on sapphire by femtosecond laser ablation. *Opt. Laser Technol.* **2020**, *132*, No. 106472.

(39) Dai, B.; Zhang, L.; Zhao, C.; Bachman, H.; Becker, R.; Mai, J.; Jiao, Z.; Li, W.; Zheng, L.; Wan, X.; Huang, T. J.; Zhuang, S.; Zhang, D. Biomimetic apposition compound eye fabricated using micro-fluidic-assisted 3D printing. *Nat. Commun.* **2021**, *12*, 6458.

(40) Li, J.; Wang, W.; Mei, X.; Pan, A.; Liu, B.; Cui, J. Rapid fabrication of microlens arrays on PMMA substrate using a microlens array by rear-side picosecond laser swelling. *Opt. Laser Eng.* **2020**, *126*, No. 105872.

(41) Hua, J.; Ren, H.; Jia, A.; Tian, Z.; Wang, L.; Juodkazis, S.; Chen, Q.; Sun, H. Convex silica microlens arrays via femtosecond laser writing. *Opt. Lett.* **2020**, *45*, 636−639.

(42) Whyman, G.; Bormashenko, E.; Stein, T. The Rigorous Derivation of Young, Cassie-Baxter and Wenzel Equations and the Analysis of the Contact Angle Hysteresis Phenomenon. *Chem. Phys.Lett.* **2008**, *450*, 355−359.

(43) Cassie, A. B. D.; Baxter, S. Wettability of Porous Surface. *Trans.Faraday Soc.* **1944**, *40*, 546−551.

(44) Yong, J.; Chen, F.; Yang, Q.; Zhang, D.; Bian, H.; Du, G.; Si, J.; Meng, X.; Hou, X. Controllable Adhesive Superhydrophobic Surfaces Based on PDMS Microwell Arrays. *Langmuir* **2013**, *29*, 3274−3279.